Original Article

Unenhanced magnetic resonance imaging of papillary thyroid carcinoma with emphasis on diffusion kurtosis imaging

Qiying Tang[1], Xinyou Liu[2], Qiuli Jiang[3], Liuhong Zhu[1], Jinhui Zhang[1], Pu-Yeh Wu[4], Ying Jiang[5#], Jianjun Zhou[1,6,7#]

[1]Department of Radiology, Xiamen Branch, Zhongshan Hospital, Fudan University, Xiamen, China; [2]Department of General Surgery, Xiamen Branch, Zhongshan Hospital, Fudan University, Xiamen, China; [3]Department of Pathology, Xiamen Branch, Zhongshan Hospital, Fudan University, Xiamen, China; [4]GE Healthcare, Beijing, China; [5]Department of General Surgery, Zhongshan Hospital, Fudan University, Shanghai, China; [6]Department of Radiology, Zhongshan Hospital, Fudan University, Shanghai, China; [7]Xiamen Clinical Research Center for Cancer Therapy, Xiamen, China

Contributions: (I) Conception and design: Q Tang, X Liu, J Zhou, Y Jiang; (II) Administrative support: J Zhou, Y Jiang; (III) Provision of study materials or patients: Y Jiang, X Liu; (IV) Collection and assembly of data: Q Tang, L Zhu, J Zhang; (V) Data analysis and interpretation: Q Tang, Q Jiang, PY Wu; (VI) Manuscript writing: All authors; (VII) Final approval of manuscript: All authors.

[#]These authors contributed equally to this work.

Correspondence to: Jianjun Zhou, MD. Department of Radiology, Xiamen Branch, Zhongshan Hospital, Fudan University, 668 Jinhu Road, Huli District, Xiamen 361015, China. Email: zhoujianjunzs@126.com; Ying Jiang, MD. Department of General Surgery, Zhongshan Hospital, Fudan University, 180 Fenglin Road, Xuhui District, Shanghai 200032, China. Email: jiang.ying3@zs-hospital.sh.cn.

Background: The aim of this study was to investigate the value of unenhanced magnetic resonance imaging (MRI) with diffusion kurtosis imaging (DKI) in diagnosing papillary thyroid carcinoma (PTC).

Methods: In all, 77 consecutive patients comprising a total of 77 thyroid nodules were enrolled in this study. Of these nodules, 41 were histopathologically confirmed PTCs and 36 were benign nodules. All patients underwent thyroid MRI including T1-weighted imaging (T1WI), T2-weighted imaging (T2WI), diffusion-weighted imaging (DWI), and DKI. All the images were assessed by 2 radiologists. The signal intensity ratio (SIR) of these nodules on T1WI and T2WI, the apparent diffusion coefficient (ADC) from DWI, and mean diffusivity (MD) and mean kurtosis (MK) from DKI were measured. Morphological features on these images were also evaluated. Univariate and multivariate logistic regression analyses were used to evaluate the value of these parameters as potential predictors of PTC.

Results: In the univariate analyses, the features that significantly indicated PTC were decreased ADC value ($P<0.001$), decreased MD value ($P<0.001$), increased MK value ($P<0.001$), younger age ($P=0.001$), female tendency ($P=0.049$), smaller tumor diameter ($P<0.001$), solid component ($P<0.001$), and irregular margin ($P<0.001$). In the multivariate analysis, decreased MD value (odds ratio =25.321; $P=0.001$), smaller diameter (odds ratio =13.751; $P=0.006$), and irregular margin (odds ratio =16.003; $P=0.003$) were independent risk factors for PTC. The combined predictor of MD, diameter, and margin showed an area under the receiver operating characteristic (ROC) curve of 0.996 in diagnosing PTC, with an optimal cutoff value of 0.69 (95.1% sensitivity, 100.0% specificity).

Conclusions: Lower MD value from DKI, smaller diameter, and irregular margin are useful predictive biomarkers for PTC.

Keywords: Thyroid neoplasms; magnetic resonance imaging (MRI); diffusion magnetic resonance imaging; differential diagnosis

Submitted Feb 26, 2022. Accepted for publication Aug 15, 2022. Published online Aug 18, 2022.
doi: 10.21037/qims-22-172
View this article at: https://dx.doi.org/10.21037/qims-22-172

Introduction

The incidence of thyroid cancer has increased rapidly worldwide (1). Papillary thyroid carcinoma (PTC) is the most common type of thyroid cancer, accounting for approximately 90% of all thyroid malignancies (2). In 2015, the American Thyroid Association (ATA) guideline proposed a "less is more" concept, which entails conducting less-extensive surgeries and less unnecessary biopsies to provide responsibly individualized therapy for patients (3). Although several international societies have developed ultrasound-based risk stratification systems to maximize the diagnostic performance of thyroid ultrasound, there are still some limitations (4). One study investigated the unnecessary thyroid nodule biopsy rates under 4 representative ultrasound risk stratification systems including the ATA, American College of Radiology (ACR), European Thyroid Association (ETA), and Korean Thyroid Association/ Korean Society of Thyroid Radiology (KTA/KSThR) (5). It was found that 25% to 55% of suspicious malignant thyroid nodules according to ultrasound diagnosis were ultimately benign after biopsy (5). This suggests that it is necessary to further improve the diagnostic accuracy of thyroid cancer, especially PTC, with noninvasive imaging modalities.

As an imaging modality with superior soft tissue contrast, magnetic resonance imaging (MRI) not only allows multiplanar assessment of the morphology of the nodules, but also provides various types of functional information. Some preliminary studies have been conducted with conventional unenhanced sequences in the assessment of PTC. In one report (6), the signal intensity of PTCs on T2-weighted imaging (T2WI) was found to be lower than that of benign nodules due to the dense fibrosis within PTCs. However, other morphological features such as tumor component (solid or cyst-solid), margin, and taller-than-wide sign were not evaluated in the study, but these are considered critical in diagnosing malignancy by ultrasound (7-9). Diffusion-weighted imaging (DWI) has been successfully used in diagnosing PTCs (6,10,11). Conventional DWI explores Gaussian diffusion distribution of free water with a mono-exponential model, which may not accurately reflect water diffusion in complex microstructures (12). In contrast, diffusion kurtosis imaging (DKI) based on non-Gaussian distribution can provide more information on the microstructural complexity of biological tissues than can conventional DWI (13,14). DKI has shown promising diagnostic value in differentiating benign from malignant tumors in various organs (15-20). To the best of our knowledge, only a single preliminary study comparing DKI to DWI in the diagnosis of thyroid nodules in a small group of patients has been conducted thus far (21). However, no previous studies have evaluated whether the combination of DKI and conventional unenhanced MRI can increase the diagnostic efficacy in PTC. Thus, the purpose of this study was to investigate the value of unenhanced MRI with DKI in patients with PTCs. We present the following article in accordance with the STARD reporting checklist (available at https://qims.amegroups.com/article/view/10.21037/qims-22-172/rc).

Methods

Patients

This prospective study was reviewed and approved by the Institutional Review Board and Ethics Committee of Xiamen Branch, Zhongshan Hospital, Fudan University. The study was conducted in accordance with the principles of the Declaration of Helsinki (as revised in 2013). Written informed consent was obtained from all participants.

Between June 2019 and July 2021, a total of 98 consecutive patients suspected of having PTC or thyroid nodules that caused compressive or structural symptoms were referred for a magnetic resonance (MR) examination to help guide individual treatment decisions. The inclusion criteria were as follows: (I) primary thyroid nodules without prior treatment, (II) pathologically confirmed thyroid nodules with surgical specimens, and (III) a nodule diameter of 10 mm or more for adequate image quality on DKI. Of the total patients, 21 were excluded after their MRI examination and surgery. The exclusion criteria were as follows: (I) patients who underwent biopsy before MRI examination (n=6), (II) a time interval between MRI examination and surgery of 2 weeks or more (n=2), (III) patients whose DKI images were inadequate for evaluation due to severe motion artifacts or magnetic susceptibility artifacts (n=8), (IV) and patients who had a nearly pure cystic nodule (n=5). Finally, 77 patients (22 males and 55

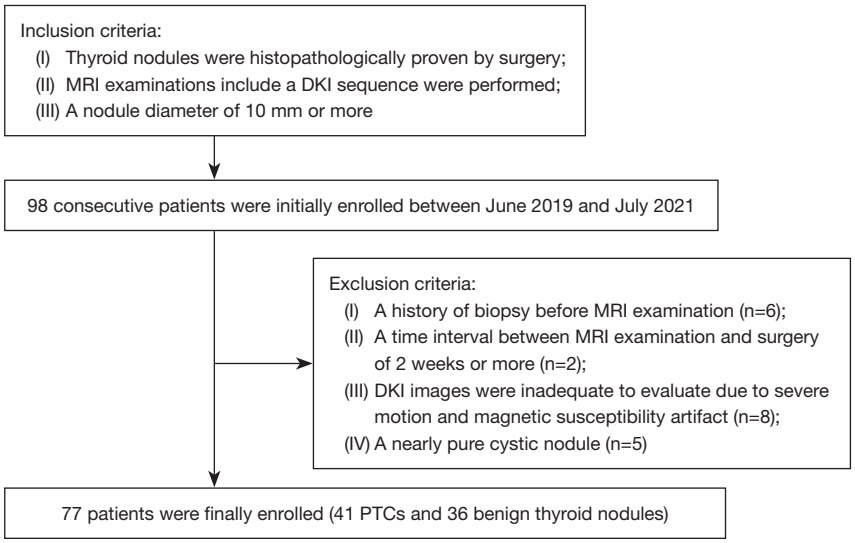

Figure 1 Flowchart of the study population. MRI, magnetic resonance imaging; DKI, diffusion kurtosis imaging; PTC, papillary thyroid carcinoma.

females; age: 46±12 years; age range: 19 to 76 years) were enrolled in our study, comprising 41 PTCs and 36 benign thyroid nodules (*Figure 1*). According to the eighth edition of the American Joint Committee on Cancer (AJCC) Tumor-Node-Metastasis (TNM) staging system (22), 36 of the 41 PTCs were stage I (87.8%) and 5 were stage II (12.2%). The distribution of pathological T classification was 34 (82.9%) with T1, 4 (9.8%) with T2, 2 (4.9%) with T3, and 1 (2.4%) with T4. The distribution of pathological N classification was 11 (26.8%) with N0, 17 (41.5%) with N1a, and 13 (31.7%) with N1b. All of the PTCs were classified as M0 in clinical M classification. Among the 36 benign thyroid nodules, there were 26 follicular adenomas, 4 nodular goiters, 4 follicular hyperplasia nodules, and 2 nodules of lymphocytic thyroiditis.

As this study applied a multivariate analysis, the sample size calculation was based on an absolute minimum ratio of 5 individuals to every variable (23). The estimated final sample size for our exploratory study was at least 60 patients, with a total of 12 variables evaluated in the study.

MRI protocol

All MRI examinations were performed on a 3.0 T scanner (Discovery MR750w, GE Healthcare, Milwaukee, WI, USA) equipped with an 8-channel head and neck combined coil. A dielectric pad was placed on the anterior portion of the neck to reduce B_1 field inhomogeneity and dielectric artifacts. The scan sequences included axial T1-weighted fast spin echo [repetition time/echo time (TR/TE) =500/9.6 ms; field of view (FOV) =22 cm × 22 cm; matrix size =256×224; slice thickness/gap =4/1 mm; number of excitations (NEX) =2], T2-weighted fast spin echo (TR/TE =2,760/85 ms; FOV =22 cm × 22 cm; matrix size =288×192; slice thickness/gap =4/1 mm; NEX =2), DWI, and DKI. The detailed parameters of the 2 diffusion sequences are summarized in *Table 1*. Spatial saturation bands were applied to remove signals from overlying fat and adjacent tissues. Postcontrast MRI was also performed in all cases but not evaluated since the focus of this study was on an unenhanced protocol.

Image analysis

All the images were assessed in consensus by 2 radiologists (JZ and QT), with 30 and 6 years of experience in head and neck imaging, respectively, who were blinded to the pathological information. The radiologists evaluated the following characteristics in MR images: (I) tumor maximum diameter; (II) location, categorized as left, right, or isthmus; (III) component, categorized as solid or cystic-solid; (IV) regular or irregular margin; and (V) taller-than-wide sign. Irregular margin was defined as either infiltrative or lobulated. Taller-than-wide sign was defined as an anteroposterior to transverse ratio of greater than 1. The anteroposterior dimension of the nodule was defined as the

Table 1 Parameters of DWI and DKI

Parameters	DWI	DKI
Pulse sequence	Single-shot EPI	Single-shot EPI
TR (ms)	4,000	3,100
TE (ms)	67.4	115.9
FOV (mm^2)	22×22	22×13
Acquisition matrix	128×128	140×84
Bandwidth (Hz/voxel)	250	166.7
Slice thickness (mm)	4	5
Gap (mm)	1	0
b values (s/mm^2)	0, 500	0, 1,000, 2,000
Directions	3	15
NEX	4	4
Scanning time	1 min 52 s	6 min 52 s

DWI, diffusion-weighted imaging; DKI, diffusion kurtosis imaging; EPI, echo planar imaging; TR, repetition time; TE, echo time; FOV, field of view; NEX, number of excitations.

diameter on the axis perpendicular to the anterior surface of the thyroid gland. The transverse dimension of the nodule was defined as the diameter on the axis perpendicular to the anteroposterior dimension. For a few cases with inconsistent results, the 2 radiologists discussed with each other to reach an agreement.

DWI and DKI were further processed by the 2 radiologists independently using FuncTool software on the GE AW4.6 Workstation to generate apparent diffusion coefficient (ADC), mean diffusivity (MD), and mean kurtosis (MK) maps. The average time required for the postprocessing was 5 min. For the thyroid nodule, a circular region of interest (ROI) was manually delineated to encompass the entire solid portion of the nodule with the most significant enhancement at the largest cross-section area, with care being taken to exclude artifacts or cystic portions. Subsequently, the ADC, MD, and MK values and the signal intensities on T1WI and T2WI were extracted from the ROI. The signal intensity ratio (SIR) on T1WI and T2WI was calculated as a ratio of the signal intensity in the thyroid nodule to that in the paraspinal muscle.

Histopathological analysis

Operative specimens of the thyroid tumors obtained after radical thyroidectomy or lobectomy were collected by a pathologist with 6 years of experience. All specimens were fixed in formalin and embedded in paraffin. The section of each thyroid tumor was stained with hematoxylin and eosin (HE). Histopathological analysis was performed using a microscope (Leica, Wetzlar, Germany) by the same pathologist who was blinded to the MRI findings.

Statistical analysis

Student's *t*-test was used for continuous variables, and the chi-squared test or Fisher exact test was used for categorical variables. Factors with a P value of less than 0.05 were enrolled into the multivariate logistic regression analysis to explore independent risk factors of PTC. The Hosmer-Lemeshow test was performed to explain the goodness of fit of the multivariate logistic model. Odds ratios and 95% confidence intervals (CIs) were calculated. Receiver operating characteristic (ROC) curve analysis was performed to evaluate the diagnostic effectiveness of the continuous variables that were statistically significant in the multivariate analysis. The area under the curve (AUC), optimal cutoff value and the corresponding sensitivity and specificity were calculated. The interobserver agreement for quantitative measurements was assessed by calculating the intraclass correlation coefficient (ICC) under the following criteria: <0.40, poor; 0.40–0.59, fair; 0.60–0.74, good; and 0.75–1.00, excellent. A 2-sided P value of less than 0.05 was considered statistically significant. All statistical analyses were performed using SPSS software (version 22.0, IBM Corp., Armonk, NY, USA) and MedCalc 19.3.1 (Mariakerke, Belgium).

Results

The clinical and MRI characteristics are summarized in *Table 2*. According to our data, patients with PTCs were younger (P=0.001) and tended to be female (P=0.049). These patients also had a smaller tumor diameter (P<0.001), a solid component (P<0.001), and an irregular margin (P<0.001) compared to those with benign nodules. No significant difference in location (P=0.853) or taller-than-wide sign (P=0.792) was noted between PTCs and benign nodules.

The T1WI SIR, T2WI SIR, ADC, MD, and MK values of all lesions are shown in *Table 3*. The ADC and MD values of PTCs were significantly lower than those of benign nodules (both P<0.001), while the MK value of PTCs was significantly higher than that of benign nodules

Table 2 Clinical and MRI characteristics of patients with PTC and benign thyroid nodules

Characteristics	PTC (n=41)	Benign (n=36)	P value
Gender			0.049
Male	8 (20%)	14 (39%)	
Female	33 (80%)	22 (61%)	
Age (years)	42±10	50±12	0.001
Tumor maximum diameter (mm)	15.07±0.57	32.08±18.16	<0.001
Location			0.853
Left	20 (49%)	16 (44%)	
Isthmus	3 (7%)	2 (6%)	
Right	18 (44%)	18 (50%)	
Component			<0.001
Solid	41 (100%)	22 (61%)	
Cystic-solid	0	14 (39%)	
Margin			<0.001
Regular	8 (20%)	34 (94%)	
Irregular	33 (80%)	2 (6%)	
Taller-than-wide sign			0.792
Yes	24 (59%)	20 (56%)	
No	17 (41%)	16 (44%)	

Data are means ± standard deviation or n (%). MRI, magnetic resonance imaging; PTC, papillary thyroid carcinoma.

Table 3 Quantitative parameters of PTC and benign thyroid nodules

MRI sequence	PTC (n=41)	Benign (n=36)	P value
SIR			
Axial T1WI	1.26±0.17	1.19±0.15	0.095
Axial T2WI	2.75±0.80	2.69±1.14	0.815
ADC ($\times10^{-3}$ mm^2/s)	1.22±0.37	1.98±0.48	<0.001
MD ($\times10^{-3}$ mm^2/s)	1.56±0.47	2.42±0.53	<0.001
MK	0.88±0.21	0.62±0.17	<0.001

The SIR was calculated for each sequence as a ratio of signal intensity of the thyroid nodule to that of the paraspinal muscle. Data are means ± standard deviation. PTC, papillary thyroid carcinoma; MRI, magnetic resonance imaging; SIR, signal intensity ratio; T1WI, T1-weighted imaging; T2WI, T2-weighted imaging; ADC, apparent diffusion coefficient; MD, mean diffusivity; MK, mean kurtosis.

(P<0.001; *Figures 2,3*). The AUCs of ADC, MD, and MK in diagnosing PTC were 0.913 (95% CI: 0.826–0.965), 0.886 (95% CI: 0.793–0.947), and 0.841 (95% CI: 0.740–0.915), respectively. The optimal cutoff values of ADC, MD, and MK in identifying PTC were 1.58×10^{-3} mm^2/s (sensitivity 87.8%, specificity 83.3%), 1.92×10^{-3} mm^2/s (sensitivity 85.4%, specificity 88.9%), and 0.78 (sensitivity 70.7%, specificity 91.7%), respectively. No significant differences in T1WI SIR (P=0.095) or T2WI SIR (P=0.815) were noted between PTCs and benign nodules. The interobserver

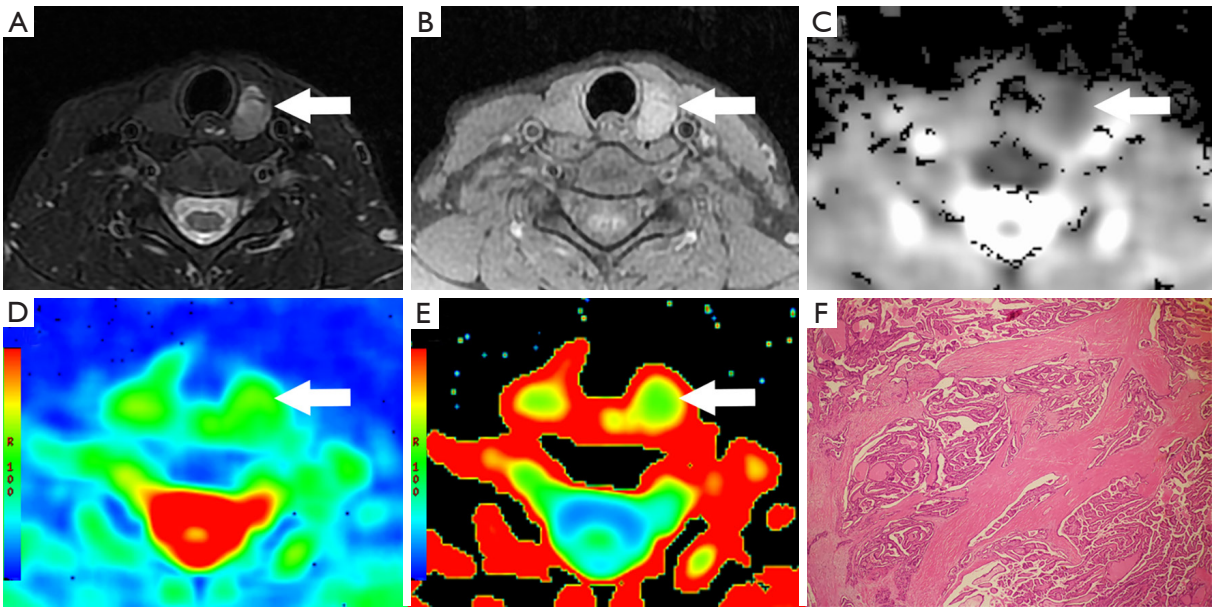

Figure 2 A 40-year-old female with PTC (arrow) in the left thyroid lobe. (A) Axial T2-WI showed a 16-mm solid nodule with locally irregular margin and a positive taller-than-wide sign: the SIR was 3.13. (B) Axial T1WI: the SIR was 1.35. (C) ADC map; ADC value $=0.93\times10^{-3}$ mm^2/s. (D) MD map; MD value $=1.59\times10^{-3}$ mm^2/s. (E) MK map; MK value =0.84. (F) Histopathological HE staining (×100). PTC, papillary thyroid carcinoma; T2WI, T2-weighted imaging; SIR, signal intensity ratio; T1WI, T1-weighted imaging; ADC, apparent diffusion coefficient; MD, mean diffusivity; MK, mean kurtosis; HE, hematoxylin and eosin.

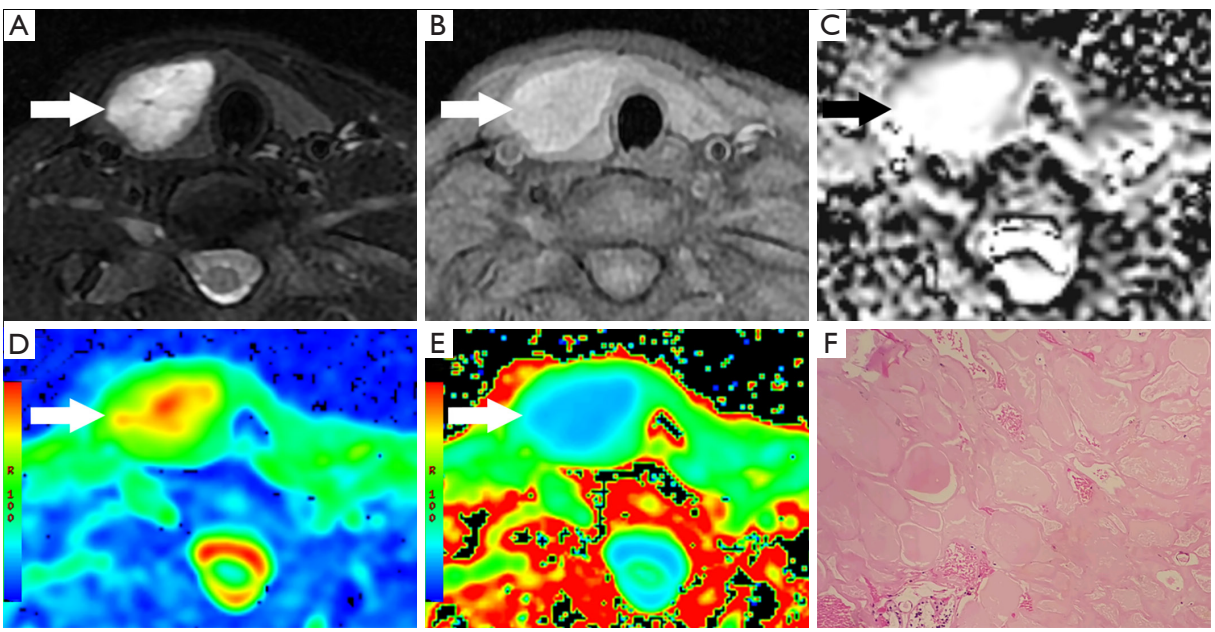

Figure 3 A 44-year-old female with thyroid adenoma (arrow) in the right thyroid lobe. (A) Axial T2-WI showed a 28-mm solid nodule with a regular margin and a negative taller-than-wide sign: the SIR was 4.58. (B) Axial T1-WI: the SIR was 1.33. (C) ADC map; ADC value $=2.78\times10^{-3}$ mm^2/s. (D) MD map; MD value $=3.05\times10^{-3}$ mm^2/s. (E) MK map; MK value =0.39. (F) Histopathological HE staining (×40). T2WI, T2-weighted imaging; SIR, signal intensity ratio; T1WI, T1-weighted imaging; ADC, apparent diffusion coefficient; MD, mean diffusivity; MK, mean kurtosis; HE, hematoxylin and eosin.

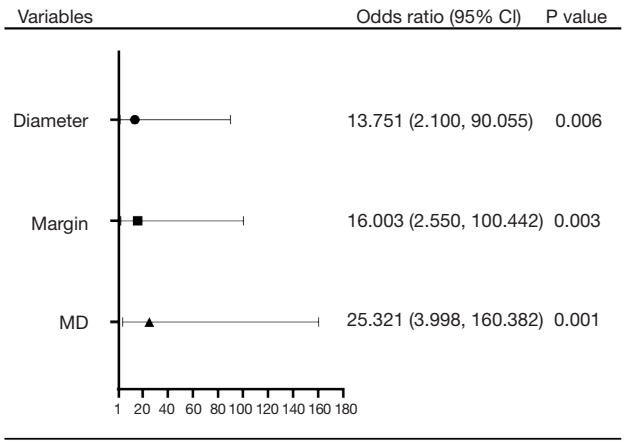

Figure 4 Binary logistic regression model for the prediction of PTC. MD, smaller diameter, and irregular margin were independent risk factors for PTC. CI, confidence interval; MD, mean diffusivity; PTC, papillary thyroid carcinoma.

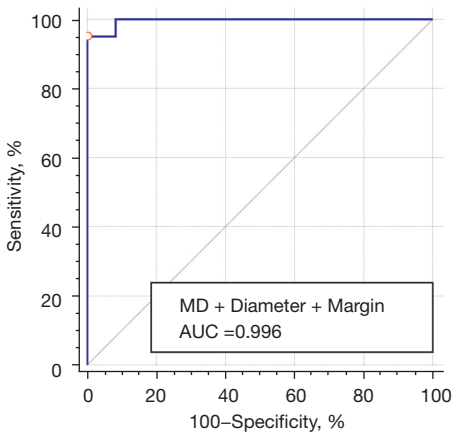

Figure 5 ROC curve of the diagnostic performance of the combined predictor of MD, diameter, and margin in identifying PTC. The AUC was 0.996 (95% CI: 0.945–1.000). The optimal cutoff value was 0.69 (sensitivity 95.1%, specificity 100.0%). MD, mean diffusivity; AUC, area under the curve; ROC, receiver operating characteristic; PTC, papillary thyroid carcinoma; CI, confidence interval.

agreements of the quantitative parameters were all excellent: T1WI SIR (ICC: 0.914; 95% CI: 0.868–0.945), T2WI SIR (ICC: 0.953; 95% CI: 0.927–0.970), ADC (ICC: 0.903; 95% CI: 0.852–0.938), MD (ICC: 0.898; 95% CI: 0.844–0.934), and MK (ICC: 0.887; 95% CI: 0.828–0.927).

In the multivariate analysis, only MD (odds ratio: 25.321; 95% CI: 3.998–160.382), smaller diameter (odds ratio: 13.751; 95% CI: 2.100–90.055), and irregular margin (odds ratio: 16.003; 95% CI: 2.550–100.442) were independent risk factors for PTC (*Figure 4*). The combined predictor of lower MD, smaller diameter, and irregular margin was generated from the logistic regression equation. The significance level of the Hosmer-Lemeshow test was 0.448, suggesting an acceptable goodness of fit of the model.

Figure 5 shows the ROC curve of the combined predictor of MD, diameter, and margin in diagnosing PTC. The AUC of the combined predictor of lower MD, smaller diameter, and irregular margin was 0.996 (95% CI: 0.945–1.000), with the optimal cutoff value of 0.69 (sensitivity 95.1%, specificity 100.0%).

Discussion

The results from our study suggest that a decreased MD value with smaller diameter and irregular margin of thyroid nodules might indicate PTC with a high predictive value. The combination of conventional unenhanced MRI and DKI can be easily acquired in clinical practice to help diagnose PTC without the need for a contrast agent.

We found a lower MD value in PTCs than in benign nodules, which was consistent with the findings reported by Shi *et al.* (21). The possible explanation for this is that the cell density of PTCs is higher than that of benign nodules, resulting in a decrease of intercellular space. Fibrosis, calcified psammoma bodies, and irregular papillary architecture might also hamper the diffusion of water molecules (12). MK describes the deviation of the water diffusion property from Gaussian behavior, which is considered to reflect the heterogeneity and irregularity of the intracellular microstructure (13,14). Shi *et al.* (21)

reported that a higher MK value in PTCs reflected a higher degree of cellular microstructural heterogeneity. However, the results of our multivariate analysis did not indicate that MK was an independent predictor for PTC although it was significantly higher in PTCs than benign nodules in the univariate analysis. The reason for this might be that, except for the different statistical approaches, the DKI protocol in our study was based on a tensor method, while Shi *et al.* (21) used a multi-b value method. These are 2 different types of DKI protocols that have been frequently used in previous studies (24-27). The tensor method applies at least 15 diffusion directions which allows better assessment of anisotropic directionality of diffusion and kurtosis behavior (14) while making the final estimates for the DKI metrics less sensitive to motion artifacts (13). Moreover, the heterogeneity of the cases in our cohort might have influenced the results, as DKI is a sequence for depicting the heterogeneity in the tissues.

In our study, irregular margin was proven as a reliable predictor of PTC among radiological features, which was consistent with previous studies (8,28-30). The histopathological mechanism of irregular margin might be the invasive and heterogeneous growing pattern of PTCs. It is important to note that an irregular margin indicates that the demarcation between nodule and parenchyma is clearly visible but demonstrates an irregular, infiltrative, or spiculated course rather than a poorly defined margin (7). In some studies, thyroid nodule size was found to be inversely related to malignancy risk, as larger nodules have lower malignancy rates (31,32). However, this has been contested by other studies (33,34). The 2015 ATA guideline and 2017 ACR Thyroid Imaging Reporting and Data System (TI-RADS) recommend diagnostic fine-needle aspiration (FNA) of the thyroid nodule based on nodule size and features of high-risk imaging on ultrasound, such as microcalcification, nodule hypoechogenicity, solid component, irregular margin, and a taller-than-wide shape (7,9). In other words, nodules with high-risk imaging features for thyroid cancer should be considered for FNA even at a smaller size, whereas nodules without these imaging features might be considered for FNA at a larger size.

Additionally, there was no significant difference in either T1WI SIR or T2WI SIR between PTCs and benign nodules in this study. In their study, Noda *et al.* (6) reported that T2WI SIRs were significantly lower in PTCs than in benign nodules. The explanation was that the presence of dense fibrous tissue within PTCs caused the reduction of T2WI SIR. In this study, a higher T2WI SIR in PTCs might be attributed to loose or edematous papillary architecture under microscopic observation, while lower T2WI SIRs in benign nodules might be attributed to the dense arrangement of follicles, coarse calcification, and fibrous tissue hyperplasia. Furthermore, various forms of degeneration and components such as stromal fibrosis, hemorrhage, calcification, and hyaline degeneration in benign nodules may also affect the T1WI signal (35,36). Accordingly, we believe that the SIR of the thyroid nodules on T1WI and T2WI might not be as useful as has been previously reported. Interestingly, taller-than-wide sign is one of the most important sonographic features in the identification of benign and malignant thyroid nodules (8,37,38), but no significant difference was found between PTCs and benign nodules in our study. Taller-than-wide sign was first described by Kim *et al.* (39), and it was speculated that benign nodules grow in normal tissue planes, whereas malignant nodules (taller-than-wide) grow across normal tissue planes. However, Yoon *et al.* (40) suggested that the mechanism of taller-than-wide sign was as follows: compared to benign masses, malignant lesions exhibit no or minimal compressibility when an ultrasound probe is applied. In their study, Seo *et al.* (41) also found the compressibility of masses to be greater in benign than in malignant lesions. In contrast to ultrasound, no compression is imposed on the thyroid tissue during MRI examination, which might partially explain our results.

There were some limitations in our study. First, the small cohort size with a limited variety of thyroid nodules is a major limitation. A larger cohort with different histological types of benign and malignant nodules is desirable to further evaluate the diagnostic criteria. Second, thyroid nodules less than 10 mm in size were not included in this study due to inadequate image quality on DKI. Since most papillary microcarcinomas (<10 mm) are indolent and nonprogressive, active surveillance is more recommended than is immediate surgery (2,42). Hence, it has a relatively small influence on the clinical decision-making process. Third, 5 mainly cystic nodules were excluded in the study due to a lack of sufficient solid components for measurement. Finally, we did not analyze the enhancement patterns of thyroid nodules. Because the emphasis of this study was on unenhanced MRI without contrast administration, a comparison between unenhanced and enhanced MRI of PTC needs to be explored in the future.

Conclusions

Lower MD values in combination with smaller diameter and irregular margin are potential predictive biomarkers for PTC. Unenhanced MRI including conventional sequences and DKI is a promising noninvasive protocol to diagnose PTC without the need for a contrast agent. Further investigations with a larger sample size of patients and specimens should be conducted to verify our results.

Acknowledgments

Funding: This work was supported by the Medical and Health Guided Project of Xiamen (No. 3502Z20199126), the Science and Technology Guided Project of Fujian Province (No. 2019D025), and the Scientific Research Cultivation and Medical Innovation Project of Fujian Province (No. 2019CXB33).

Footnote

Reporting Checklist: The authors have completed the STARD reporting checklist. Available at https://qims.amegroups.com/article/view/10.21037/qims-22-172/rc

Conflicts of Interest: All authors have completed the ICMJE uniform disclosure form (available at https://qims.amegroups.com/article/view/10.21037/qims-22-172/coif). PYW is an employee of GE Healthcare and was involved in the data postprocessing and interpretation of this study. The other authors have no conflicts of interest to declare.

Ethical Statement: The authors are accountable for all aspects of the work in ensuring that questions related to the accuracy or integrity of any part of the work are appropriately investigated and resolved. The study was conducted in accordance with the Declaration of Helsinki (as revised in 2013). This prospective study was approved by the Institutional Review Board of Xiamen Branch, Zhongshan Hospital, Fudan University, and written informed consent was obtained from all patients.

References

1. Vaccarella S, Dal Maso L, Laversanne M, Bray F, Plummer M, Franceschi S. The Impact of Diagnostic Changes on the Rise in Thyroid Cancer Incidence: A Population-Based Study in Selected High-Resource Countries. Thyroid 2015;25:1127-36.
2. Oda H, Miyauchi A, Ito Y, Yoshioka K, Nakayama A, Sasai H, Masuoka H, Yabuta T, Fukushima M, Higashiyama T, Kihara M, Kobayashi K, Miya A. Incidences of Unfavorable Events in the Management of Low-Risk Papillary Microcarcinoma of the Thyroid by Active Surveillance Versus Immediate Surgery. Thyroid 2016;26:150-5.
3. Kim BW, Yousman W, Wong WX, Cheng C, McAninch EA. Less is More: Comparing the 2015 and 2009 American Thyroid Association Guidelines for Thyroid Nodules and Cancer. Thyroid 2016;26:759-64.
4. Zhu H, Yang Y, Wu S, Chen K, Luo H, Huang J. Diagnostic performance of US-based FNAB criteria of the 2020 Chinese guideline for malignant thyroid nodules: comparison with the 2017 American College of Radiology guideline, the 2015 American Thyroid Association guideline, and the 2016 Korean Thyroid Association guideline. Quant Imaging Med Surg 2021;11:3604-18.
5. Kim PH, Suh CH, Baek JH, Chung SR, Choi YJ, Lee JH. Unnecessary thyroid nodule biopsy rates under four ultrasound risk stratification systems: a systematic review and meta-analysis. Eur Radiol 2021;31:2877-85.
6. Noda Y, Kanematsu M, Goshima S, Kondo H, Watanabe H, Kawada H, Bae KT. MRI of the thyroid for differential diagnosis of benign thyroid nodules and papillary carcinomas. AJR Am J Roentgenol 2015;204:W332-5.
7. Haugen BR, Alexander EK, Bible KC, Doherty GM, Mandel SJ, Nikiforov YE, Pacini F, Randolph GW, Sawka AM, Schlumberger M, Schuff KG, Sherman SI, Sosa JA, Steward DL, Tuttle RM, Wartofsky L. 2015 American Thyroid Association Management Guidelines for Adult Patients with Thyroid Nodules and Differentiated Thyroid Cancer: The American Thyroid Association Guidelines Task Force on Thyroid Nodules and Differentiated Thyroid Cancer. Thyroid 2016;26:1-133.
8. Moon WJ, Jung SL, Lee JH, Na DG, Baek JH, Lee YH, Kim J, Kim HS, Byun JS, Lee DH; Thyroid Study Group, Korean Society of Neuro- and Head and Neck

Radiology. Benign and malignant thyroid nodules: US differentiation—multicenter retrospective study. Radiology 2008;247:762-70.
9. Tessler FN, Middleton WD, Grant EG, Hoang JK, Berland LL, Teefey SA, Cronan JJ, Beland MD, Desser TS, Frates MC, Hammers LW, Hamper UM, Langer JE, Reading CC, Scoutt LM, Stavros AT. ACR Thyroid Imaging, Reporting and Data System (TI-RADS): White Paper of the ACR TI-RADS Committee. J Am Coll Radiol 2017;14:587-95.
10. Erdem G, Erdem T, Muammer H, Mutlu DY, Firat AK, Sahin I, Alkan A. Diffusion-weighted images differentiate benign from malignant thyroid nodules. J Magn Reson Imaging 2010;31:94-100.
11. Kong W, Yue X, Ren J, Tao X. A comparative analysis of diffusion-weighted imaging and ultrasound in thyroid nodules. BMC Med Imaging 2019;19:92.
12. Le Bihan D. Apparent diffusion coefficient and beyond: what diffusion MR imaging can tell us about tissue structure. Radiology 2013;268:318-22.
13. Jensen JH, Helpern JA. MRI quantification of non-Gaussian water diffusion by kurtosis analysis. NMR Biomed 2010;23:698-710.
14. Jensen JH, Helpern JA, Ramani A, Lu H, Kaczynski K. Diffusional kurtosis imaging: the quantification of non-gaussian water diffusion by means of magnetic resonance imaging. Magn Reson Med 2005;53:1432-40.
15. Ding Y, Tan Q, Mao W, Dai C, Hu X, Hou J, Zeng M, Zhou J. Differentiating between malignant and benign renal tumors: do IVIM and diffusion kurtosis imaging perform better than DWI? Eur Radiol 2019;29:6930-9.
16. Jiang JX, Tang ZH, Zhong YF, Qiang JW. Diffusion kurtosis imaging for differentiating between the benign and malignant sinonasal lesions. J Magn Reson Imaging 2017;45:1446-54.
17. Sun K, Chen X, Chai W, Fei X, Fu C, Yan X, Zhan Y, Chen K, Shen K, Yan F. Breast Cancer: Diffusion Kurtosis MR Imaging-Diagnostic Accuracy and Correlation with Clinical-Pathologic Factors. Radiology 2015;277:46-55.
18. Wan Q, Deng YS, Lei Q, Bao YY, Wang YZ, Zhou JX, Zou Q, Li XC. Differentiating between malignant and benign solid solitary pulmonary lesions: are intravoxel incoherent motion and diffusion kurtosis imaging superior to conventional diffusion-weighted imaging? Eur Radiol 2019;29:1607-15.
19. Mokry T, Mlynarska-Bujny A, Kuder TA, Hasse FC, Hog R, Wallwiener M, Dinkic C, Brucker J, Sinn P, Gnirs R, Kauczor HU, Schlemmer HP, Rom J, Bickelhaupt S. Ultra-High-b-Value Kurtosis Imaging for Noninvasive Tissue Characterization of Ovarian Lesions. Radiology 2020;296:358-69.
20. Chen W, Li L, Yan Z, Hu S, Feng J, Liu G, Liu B, Liu X. Three-dimension amide proton transfer MRI of rectal adenocarcinoma: correlation with pathologic prognostic factors and comparison with diffusion kurtosis imaging. Eur Radiol 2021;31:3286-96.
21. Shi RY, Yao QY, Zhou QY, Lu Q, Suo ST, Chen J, Zheng WJ, Dai YM, Wu LM, Xu JR. Preliminary study of diffusion kurtosis imaging in thyroid nodules and its histopathologic correlation. Eur Radiol 2017;27:4710-20.
22. Amin MB, Greene FL, Edge SB, Compton CC, Gershenwald JE, Brookland RK, Meyer L, Gress DM, Byrd DR, Winchester DP. The Eighth Edition AJCC Cancer Staging Manual: Continuing to build a bridge from a population-based to a more "personalized" approach to cancer staging. CA Cancer J Clin 2017;67:93-9.
23. Everitt BS. Multivariate analysis: the need for data, and other problems. Br J Psychiatry 1975;126:237-40.
24. Cho E, Baek HJ, Szczepankiewicz F, An HJ, Jung EJ, Lee HJ, Lee J, Gho SM. Clinical experience of tensor-valued diffusion encoding for microstructure imaging by diffusional variance decomposition in patients with breast cancer. Quant Imaging Med Surg 2022;12:2002-17.
25. Roethke MC, Kuder TA, Kuru TH, Fenchel M, Hadaschik BA, Laun FB, Schlemmer HP, Stieltjes B. Evaluation of Diffusion Kurtosis Imaging Versus Standard Diffusion Imaging for Detection and Grading of Peripheral Zone Prostate Cancer. Invest Radiol 2015;50:483-9.
26. Wang F, Chen HG, Zhang RY, Jin D, Xu SS, Wu GY, Xu JR. Diffusion kurtosis imaging to assess correlations with clinicopathologic factors for bladder cancer: a comparison between the multi-b value method and the tensor method. Eur Radiol 2019;29:4447-55.
27. Zhang Q, Yu X, Ouyang H, Zhang J, Chen S, Xie L, Zhao X. Whole-tumor texture model based on diffusion kurtosis imaging for assessing cervical cancer: a preliminary study. Eur Radiol 2021;31:5576-85.
28. Gul K, Ersoy R, Dirikoc A, Korukluoglu B, Ersoy PE, Aydin R, Ugras SN, Belenli OK, Cakir B. Ultrasonographic evaluation of thyroid nodules: comparison of ultrasonographic, cytological, and histopathological findings. Endocrine 2009;36:464-72.
29. Kwak JY, Han KH, Yoon JH, Moon HJ, Son EJ, Park SH, Jung HK, Choi JS, Kim BM, Kim EK. Thyroid imaging reporting and data system for US features of nodules: a step in establishing better stratification of cancer risk.

Radiology 2011;260:892-9.
30. Wang H, Wei R, Liu W, Chen Y, Song B. Diagnostic efficacy of multiple MRI parameters in differentiating benign vs. malignant thyroid nodules. BMC Med Imaging 2018;18:50.
31. Cavallo A, Johnson DN, White MG, Siddiqui S, Antic T, Mathew M, Grogan RH, Angelos P, Kaplan EL, Cipriani NA. Thyroid Nodule Size at Ultrasound as a Predictor of Malignancy and Final Pathologic Size. Thyroid 2017;27:641-50.
32. Shayganfar A, Hashemi P, Esfahani MM, Ghanei AM, Moghadam NA, Ebrahimian S. Prediction of thyroid nodule malignancy using thyroid imaging reporting and data system (TIRADS) and nodule size. Clin Imaging 2020;60:222-7.
33. Chung SR, Baek JH, Choi YJ, Sung TY, Song DE, Kim TY, Lee JH. The relationship of thyroid nodule size on malignancy risk according to histological type of thyroid cancer. Acta Radiol 2020;61:620-8.
34. Jinih M, Faisal F, Abdalla K, Majeed M, Achakzai AA, Heffron C, McCarthy J, Redmond HP. Association between thyroid nodule size and malignancy rate. Ann R Coll Surg Engl 2020;102:43-8.
35. Luetkens JA, Klein S, Träber F, Schmeel FC, Sprinkart AM, Kuetting DLR, Block W, Uschner FE, Schierwagen R, Hittatiya K, Kristiansen G, Gieseke J, Schild HH, Trebicka J, Kukuk GM. Quantification of Liver Fibrosis at T1 and T2 Mapping with Extracellular Volume Fraction MRI: Preclinical Results. Radiology 2018;288:748-54.
36. Lloyd RV, Osamura RY, Klöppel G, Rosai J. WHO Classification of Tumours of Endocrine Organs. 4th edition. Lyon: IARC, 2017.
37. Cappelli C, Castellano M, Pirola I, Gandossi E, De Martino E, Cumetti D, Agosti B, Rosei EA. Thyroid nodule shape suggests malignancy. Eur J Endocrinol 2006;155:27-31.
38. Kim JY, Lee CH, Kim SY, Jeon WK, Kang JH, An SK, Jun WS. Radiologic and pathologic findings of nonpalpable thyroid carcinomas detected by ultrasonography in a medical screening center. J Ultrasound Med 2008;27:215-23.
39. Kim EK, Park CS, Chung WY, Oh KK, Kim DI, Lee JT, Yoo HS. New sonographic criteria for recommending fine-needle aspiration biopsy of nonpalpable solid nodules of the thyroid. AJR Am J Roentgenol 2002;178:687-91.
40. Yoon SJ, Yoon DY, Chang SK, Seo YL, Yun EJ, Choi CS, Bae SH. "Taller-than-wide sign" of thyroid malignancy: comparison between ultrasound and CT. AJR Am J Roentgenol 2010;194:W420-4.
41. Seo YL, Yoon DY, Yoon SJ, Lim KJ, Yun EJ, Choi CS, Bae SH. Compressibility of thyroid masses: a sonographic sign differentiating benign from malignant lesions? AJR Am J Roentgenol 2012;198:434-8.
42. Ito Y, Miyauchi A, Kihara M, Higashiyama T, Kobayashi K, Miya A. Patient age is significantly related to the progression of papillary microcarcinoma of the thyroid under observation. Thyroid 2014;24:27-34.

Cite this article as: Tang Q, Liu X, Jiang Q, Zhu L, Zhang J, Wu PY, Jiang Y, Zhou J. Unenhanced magnetic resonance imaging of papillary thyroid carcinoma with emphasis on diffusion kurtosis imaging. Quant Imaging Med Surg 2023;13(4):2697-2707. doi: 10.21037/qims-22-172

